CHAPTER 9

RESIDUAL STRESS IN LASER POWDER BED FUSION

Lameck Mugwagwa [1], Ina Yadroitsava [1], Washington Makoana [1,2], Igor Yadroitsev [1]

[1] Department of Mechanical and Mechatronic Engineering, Central University of Technology, Free State, South Africa
lmugwagwa@cut.ac.za

[2] Council for Scientific and Industrial Research, National Laser Centre, Pretoria, South Africa

Abstract

Laser powder bed fusion (L-PBF) has great prospects for biomedical, automotive, aerospace and other high-tech industry sectors due to its manufacturing flexibility and design freedom. However, several factors that include high residual stresses, random porosity and dimensional accuracy can affect the quality of parts and hamper L-PBF progress and widespread industrial applications. Residual stresses are inherent in laser-based processing, and focused studies to control these stresses are topical. Thermal and mechanical post-processing methods, such as stress-relief heat treatment and machining, can relieve residual stresses but cannot reverse in situ stress-induced distortions or cracking. Thus, in situ stress relief remains an attractive option/complement for managing the effect of residual stress on part strength, surface integrity, and dimensional accuracy. Better still, combining in situ and post-processing stress-relief techniques could be a more effective approach to residual stress control. This chapter presents a detailed analysis of the residual stress control techniques that can be applied in L-PBF. Recommendations for effective evaluation and appropriate selection of residual stress management techniques are outlined.

Keywords: additive manufacturing; laser powder bed fusion; residual stress; defects; distortions; in situ control; post processing

9.1. INTRODUCTION

Residual stresses in an object are those stresses that remain in the object when all external forces, apart from gravity, do not act on this object. Since residual stress is balanced in the object, the presence of tensile stress (positive in sign) in one part is compensated by compressive stress (negative) in other parts of this object. The primary reasons for residual stresses are non-uniform plastic deformations through the cross-section during mechanical processing, phase transformations and thermal gradients, i.e. residual stresses have mechanical, chemical and thermal origins.

Residual stresses can be introduced during manufacturing, during in-service repair or modification, during operation or even during part installation, assembly procedures or occasional overloads, etc. For example, residual stress in drilling is introduced by plastic deformation due to the removal of chips, thermal stress introduced by heating and possible phase transformation if the temperature is sufficient. In practice, no component is entirely free of residual stress, which originates during processing.

Residual stresses can be divided into the following length scales: Type I, II and III (Figure 9.1). Type I are macro-stresses which equilibrate over large distances or dimensions (size of the part or structure). Macro-stresses may be introduced by non-uniform plastic deformation due to material processing such as shot peening, forging, milling, bending, welding, different surface treatments (plating, enameling, coatings, hardening), or by heating or cooling (for example, quenching heat treatment procedure). Residual stress can also be introduced by differing thermal expansion coefficients and mechanical mismatching of varying components of composites as multiphase materials, ceramic coatings, etc. Type I residual stress can also occur under material load: e.g. mechanical loading, thermal temperature fields or chemical changes during operation.

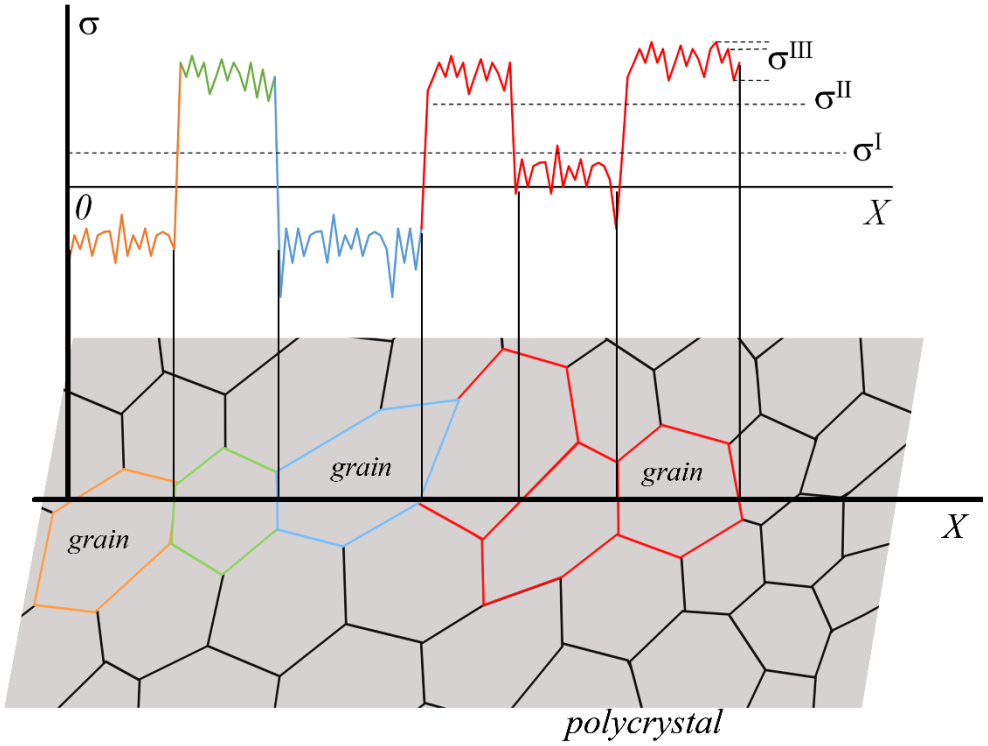

Figure 9.1. Residual stress in polycrystalline material categorized according to length scales.

Type II are micro-intergranular stresses that equilibrate over a length relating to the grain dimensions, usually 3–10 times that of the grain size (Totten, Howes and Inoue, 2002). These stresses are caused by differences in microstructure of polycrystalline materials when phase transformation has taken place in a multiphase material or in a single phase material when anisotropy of grains occurs. An example is thermal stresses in metal-matrix composites.

Type III are stresses that are present within a grain and typically includes stresses due to coherency at interfaces and dislocation stress fields (Withers and Bhadeshia, 2001).

The effects of residual stress may be either beneficial or detrimental, depending upon the magnitude, size and distribution of the stress with respect to the load-induced stresses (Withers and Bhadeshia, 2001a, 2001b). For example, tensile residual stress near the surface has a detrimental influence on fatigue and corrosive properties, especially if this part is also subjected to tensile load during operation. So, in parts with residual stresses, not only is loading magnitude critical, but also direction.

All metal part manufacturing methods, such as die and investment castings, sintering, machining, metal injection molding and additive manufacturing (AM), introduce residual stresses into the manufactured object. During welding or powder bed fusion, residual stress can be generated by shrinkage, deformations during processing, temperature variations and phase transformations. This chapter provides metal AM researchers with important information regarding residual stress measurements, their origins, effects in L-PBF objects, the available residual stress mitigation methods and how such methods impact on the end product quality characteristics. Furthermore, the implications of the various residual stress management approaches are discussed, bearing in mind the interdependent, competing or conflicting effects of the interventions on residual stress and other process outcomes such as density, surface quality, manufacturing time and cost.

9.2. RESIDUAL STRESS MEASUREMENTS

The effective control of residual stress and qualification of the manufacturing process for various applications depend on accurate measurement of the residual stresses. Evaluation of residual stress is done by means of measuring strain using a variety of methods and using the measured strain to calculate stress based on variations of Hooke’s laws. Alternatively, residual stress can be evaluated qualitatively by measuring distortions that emanate from them. Two broad approaches can be used to evaluate residual stress – non-destructive and destructive methods. Detailed explanation of measurement techniques of residual stress can be found in (Withers and Bhadeshia, 2001a). In this section, some frequently used methods are shortly described.

9.2.1. Destructive methods

All destructive and semi-destructive methods of measuring residual stress work on the same principle of inducing stress relaxation followed by strain or deflection measurements. Thus, destructive techniques are also called relaxation methods (Schajer, 2010). Stress relaxation can be achieved by cutting or removing some material from the specimen. Methods that rely on macro-deflection measurement are purely qualitative, although FE methods can be used to calculate the actual stress responsible for the distortion. However, no standard geometries exist to allow universally acceptable and reliable evaluation. For this reason, deflection-based methods have largely remained qualitative.

The ***hole drilling method*** is one of the most common methods in which strain gages are used to measure the strain that results from stress relaxation after material removal from a specimen. This method has been used to evaluate residual stress in a range of L-PBF metal alloys including Ti6Al4V and AlSi10Mg (Knowles, Becker and Tait, 2012; Salmi *et al.*, 2017). In this method, a small hole is drilled in the center of a strain gage rosette attached to the surface of the component to be measured. The action of drilling the hole relieves locked-up stress and this is accompanied by a change in the strain state, which can easily be measured using the strain gage (Figure 9.2a). The strain change is then used to compute the equivalent stress state through a series of equations, as specified in ASTM E837-08. The accuracy of this method depends on surface roughness, levels of stress, correct alignment for drilling, selection of incremental hole depths, gage placements, etc. Similar to the hole drilling method, other relaxation techniques such as indentation or cutting of a long slit (so-called "slitting method", or "***crack compliance method***", Figure 9.2b) are used for investigation of residual stress with strain gages (Schajer, 2013).

Digital image correlation (DIC) is a widely used method for measuring residual stress in L-PBF-manufactured components. DIC acquires strain data from images by comparing the location of a subset or block of pixels on a test piece before and after deformation (Lord, Penn and Whitehead, 2008). The image taken before deformation is the reference image and several other images can be taken at different stages of the deformation. For example, when testing the hardness of a material which suffers from residual stress, the indentation may deform to a certain extent (or the residual stress may influence the hardness number). The magnitude of the deformity may be compared with that of a non-stressed part; the change in area of the indentation could be converted to strain which then can be converted to a stress value using Hooke's law (Totten, Howes and Inoue, 2002; Song et al., 2014).

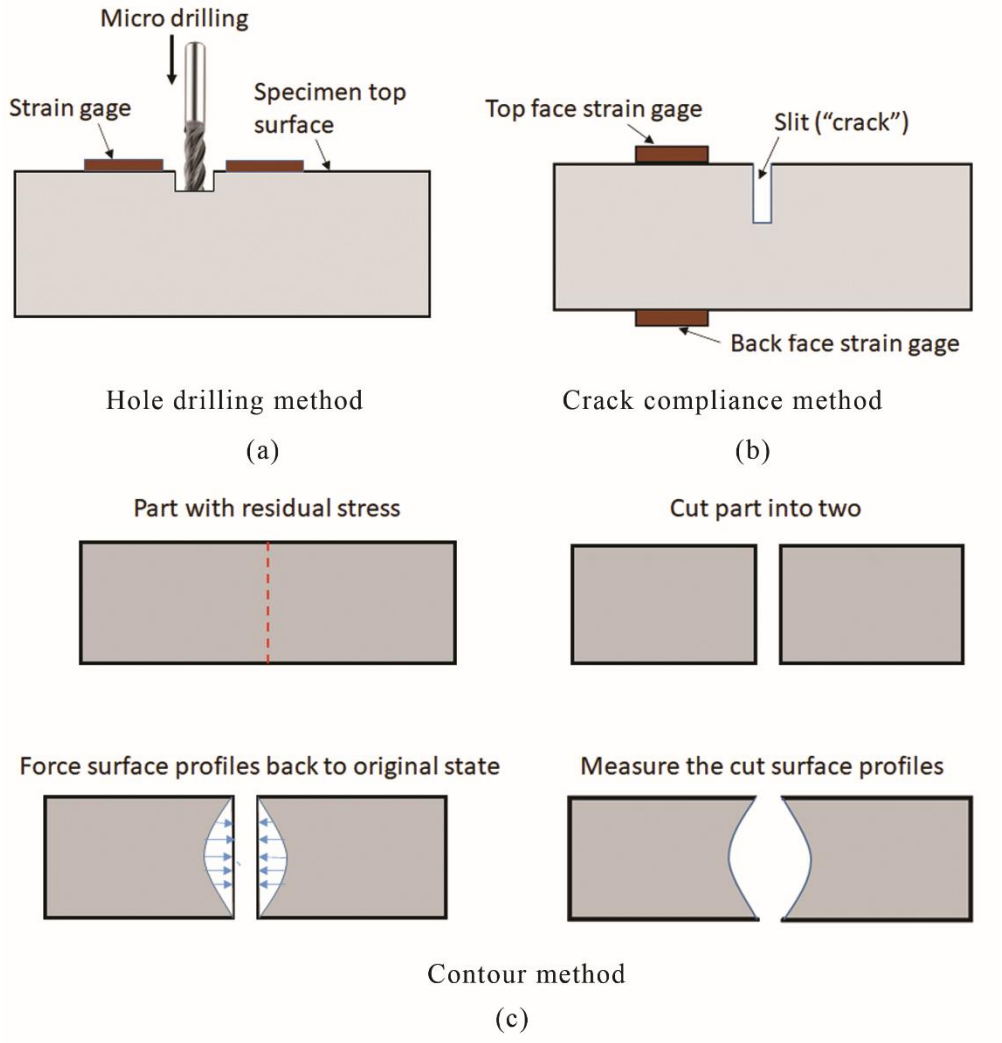

Figure 9.2. Measurements of residual stress by hole drilling (a), crack compliance method (b) and contour method (c).

Residual stress can also be estimated using the ***contour method*** **(Figure 9.2c)**. The component under investigation is carefully cut in two using non-stress-inducing methods such as wire electric discharge machining. When the surface of the plane of interest is cut, residual stress is partially relieved, causing deformations or deviations of the cut surfaces from the expected surface profile. These surface distortions can be measured using a touch probe of a coordinate measurement machine or a laser profilometer. The stress state is determined with the aid of FE modeling by superimposing the partially relaxed stress state with the stress change, after forcing back the deformations to the original state before cutting (Ahmad et al., 2018; Robinson et al., 2018). The contour method only measures the stress component normal to the cut. A multi-axial contour method has been developed to determine 3D stress maps by

introducing multiple cuts along different planes (or axes) of interest to measure the stresses normal to the cut planes (Pagliaro et al., 2010).

The ***curvature method*** is a technique in which deflection (curl-up angle) stemming from residual stress is measured for a bridge-like, thin plate or cantilever structure (Figure 9.3). A specially shaped part is built on a base plate and later cut off. After removal from the base plate, the part can curl up through an angle which can be measured (Kruth et al., 2010, 2012; Vrancken et al., 2013; Buchbinder et al., 2014; Liang et al., 2020) Simulations are then used to calculate the actual residual stress corresponding to this measured curl-up angle. A major weakness of methods that rely on distortion and localized strain measurement to calculate residual stress is that the stress relaxation does not necessarily release all the stress from the component. As a result, the calculated stress is not necessarily representative of the actual state of stress in the part. Therefore, methods that can profile the residual stress for greater part volume are preferred.

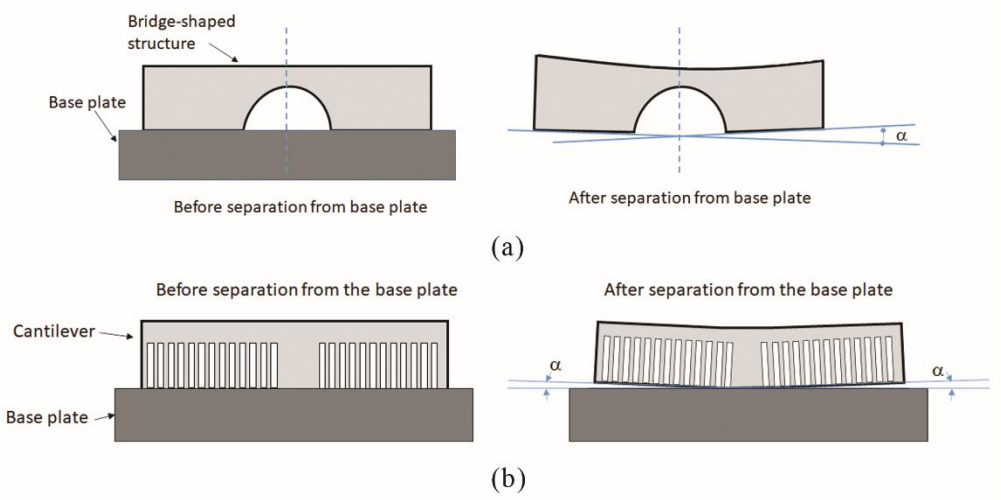

Figure 9.3. Measurements of residual stress by curvature method: with bridges (a) and with cantilevers (b). Deformation after separation from the base plate and curl-up angle α are shown.

9.2.2. Non-destructive techniques

Non-destructive techniques for residual stress measurement are largely based on diffraction and acoustic principles (see also chapter 10). Common non-destructive residual stress measurement methods are neutron and X-ray diffraction (XRD). Less common methods include synchrotron radiation based XRD, ultrasonic and electromagnetic techniques. A comprehensive review on ultrasonic testing of residual stress for AM parts was done recently by Acevedo et al. (2020).

The diffraction methods basically make use of the inter-atomic *d*-spacing as a built-in strain gage. ***Neutron diffraction*** measurement of residual stress depends on strain evaluation through measurement of the change in crystallographic lattice spacing using Bragg's law of diffraction (Figure 9.4) and utilizing Hooke's laws to calculate the subsurface residual stress. Due to the high penetration power of neutrons, neutron diffraction is capable of measuring volumetric residual stress in thick specimens. When a beam of neutrons impinges on the surface of a stressed material, the atomic planes will diffract the neutrons at a diffraction angle 2θ. The lattice plane spacing is then calculated from employing Bragg's law of constructive interference according to:

$$n\lambda = 2dsin\theta \tag{1}$$

where n and λ represent the order and wavelength of the neutron radiation respectively and *d* is a lattice spacing (Figure 9.4).

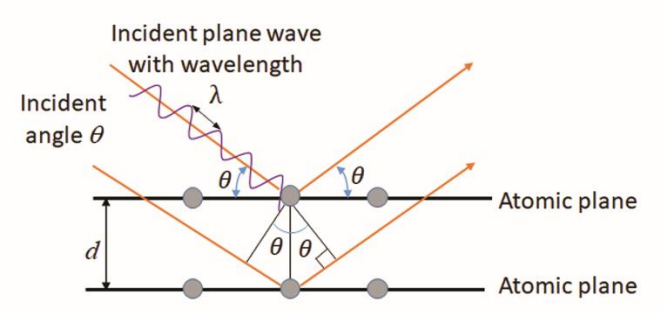

Figure 9.4. Bragg diffraction.

The residual strain ε can be calculated using Equation 2 based on the change of lattice spacing from the normal spacing (d_0) to a new value (d) when the material is under stress.

$$\varepsilon = \frac{d-d_0}{d_0} \tag{2}$$

The strains are converted to stresses by applying Hooke's law with the incorporation of the appropriate constants, that is, the material's modulus of elasticity, Poisson's ratio and the diffraction elastic constants for the *hkl* family of lattice planes.

Unfortunately, neutron diffraction is expensive and time consuming and facilities are limited. A cheaper, quicker, more accessible and more widely used option for residual stress measurement is the ***X-ray diffraction*** (XRD) method. XRD has a working principle similar to neutron diffraction, except that X-rays have less penetrating power than neutrons. Due to the lower

penetration power of X-rays in metal, XRD is limited to surface and near surface stress measurement – for typical laboratory devices. The surfaces to be analyzed must be free from dirt and roughness, so light electro-polishing is usually applied (Withers and Bhadeshia, 2001a). Great care must be taken to ensure that no residual stress or plastic deformation is induced during surface preparation.

9.3. EFFECTS AND ORIGINS OF RESIDUAL STRESS IN L-PBF

The use of a fast-moving laser beam with high power leads to rapid heating, melting, solidifying and cooling cycles during L-PBF. Large thermal gradients and layer-by-layer manufacturing using powder result in high anisotropic residual stress, specific microstructure (Chapter 13), random porosity (Chapter 6) and limited accuracy of fine structural units of L-PBF parts (Chapters 5, 7, 16). As-built L-PBF materials have anisotropic non-equilibrium microstructure that is a result of high cooling rates and the layer-wise nature of this process. In some materials, the resulting microstructure in combination with high residual stress, can lead to cracking during processing (Qiu et al., 2019; Zhang et al., 2020). Some of the common defects associated with residual stress in L-PBF during processing are shown in Figure 9.5: excessive residual stress leads to macro- and microcracking, deformation and delamination from the base plate or supports during part manufacturing (Figure 9.5 a-c). When parts delaminate or deform during processing, the structures elevate above the powder bed top surface and come into contact with the recoater, which can cause damage to the parts and the entire deposition system. Even the slightest contact between the part and the recoater can cause the part to flex and then relax, causing the part to act as a spring which moves or shoots powder away from the contact area which leads to defects (Figure 9.5d).

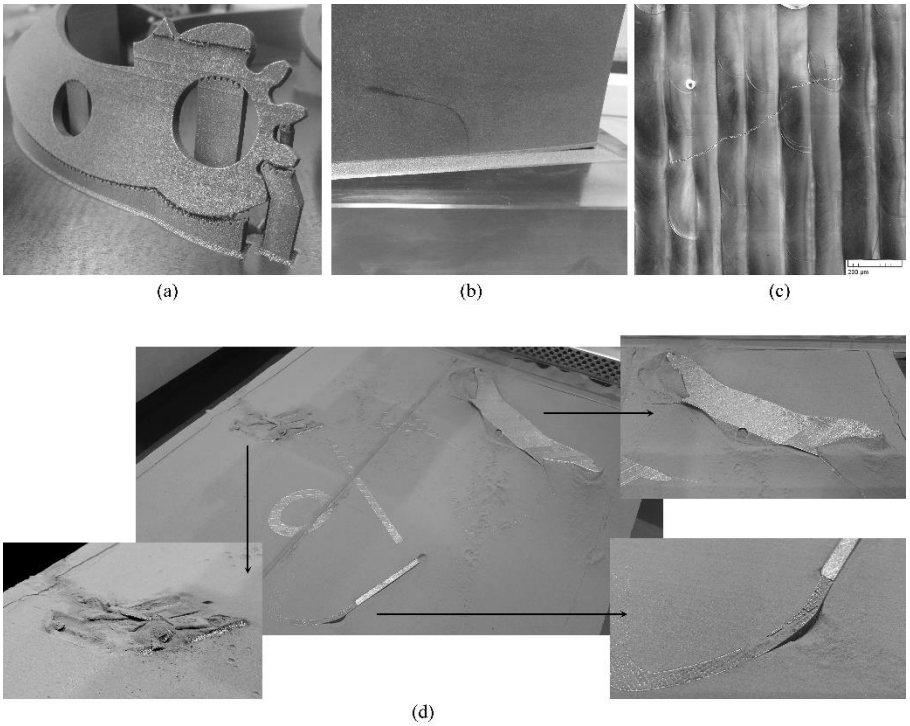

Figure 9.5. Defects in L-PBF parts during manufacturing: (a) delamination from the supports and deformation during processing Ti6L4V alloy; (b) delamination from the base plate and macrocracking in massive Ti6L4V solid sample; (c) cracks at the top surface of Ti-Al single layer; (d) general view of redistribution of powder bed during manufacturing: delamination from support and deformation resulting in contact with recoater: deformation of massive part (top image in d) and vibration of fine parts (bottom images)

Where the distortion does not lead to process disruption, more defects are still likely to occur owing to the resultant uneven powder distribution and non-homogenous powder layers that provoke porosity and dimensional errors (du Plessis et al., 2018; Bartlett and Li, 2019). Furthermore, if delamination, cracking or distortions do not occur during processing, as-built L-PBF parts have been known to deform after being removed from the base plate due to residual stress. Residual stress does not only impact the technical capabilities of the L-PBF processes but can severely offset the economic gains that could be associated with AM (see chapter 22). L-PBF parts have to be heat-treated, machined, etc. in order to reduce residual stress. Inevitably, this additional post-processing results in loss of productive time and hampers the efficient use of manufacturing resources. When the effects of residual stress cause integrity problems such as cracks and these cannot be reversed by post-processing methods, the parts must be taken out of service. To qualify L-PBF as a process of choice for industrial applications that have stringent quality requirements, residual stress needs to be controlled.

The effect of residual stress on dimensional and form deviations has been widely demonstrated in Neugebauer et al. (2014), Yadroitsava and Yadroitsev (2015), and Debroy et al. (2018). Stress-induced distortion by only a couple of micrometers could be detrimental to the possible industrial application. The fatigue and corrosion behaviors also depend on the nature and values of residual stress (Lu, 2002; Vrancken et al., 2014; Örnek, 2018; Cruz et al., 2020), see Chapters 14-15 on structural integrity and fatigue properties. As mentioned earlier, specific microstructure that develops during L-PBF, in cooperation with high stresses, can induce cracking and delamination in the final part (Kempen *et al.*, 2013; DebRoy *et al.*, 2018).

A development of residual stress in L-PBF in terms of heating/cooling cycles ("temperature gradient mechanism") and shrinkage due to the thermal contraction and elastic-plastic behavior of the material at different temperatures ("cool-down phase model") was described in (Shiomi *et al.*, 2004; Mercelis and J. P. Kruth, 2006). First, the irradiated layers expand due to the heating effect of the laser beam (Figure 9.6). However, the solid underlying substrate (or a previously processed layer) restricts this expansion resulting in an overall compressive stress-strain condition at the top surface. Then, after the removal of the laser beam, the material tends to cool down and to shrink. Again, this shrinkage is confined by the partial elastic-plastic deformation set up during the heating cycle, leading to an overall tensile stress state in the upper surface of the solidified material.

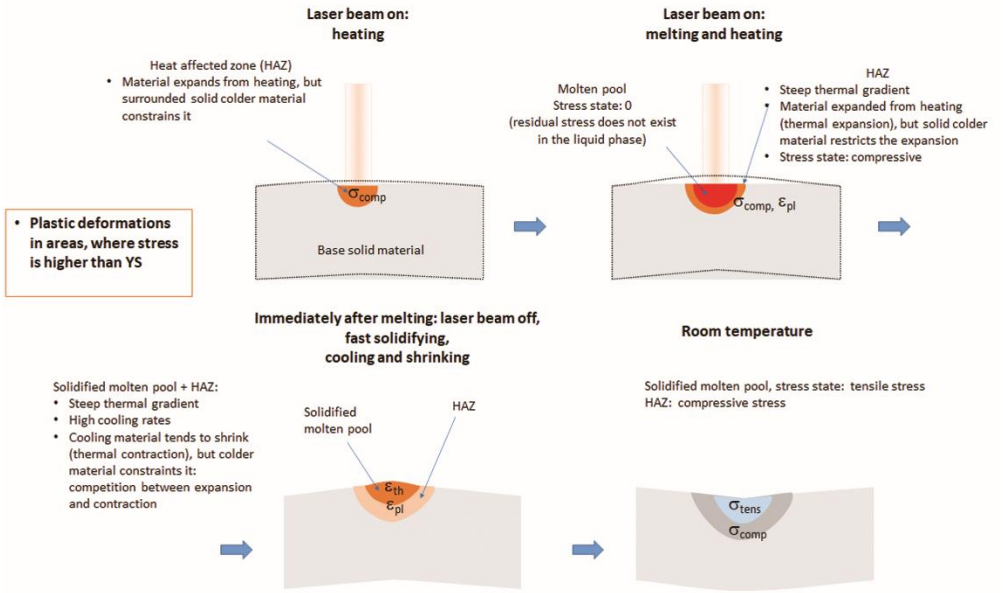

Figure 9.6. Residual stress development during L-PBF

During L-PBF manufacturing, different process parameters and scanning strategies are used for different areas of the part and the geometry and the shape of the melt pool vary significantly. The temperature gradients and the amount of material involved also vary, which makes residual stress distribution quite complex: its values depend on many factors. Cooling down and solidification commences when the laser beam leaves the irradiated zone (Figure 9.6). However, the contraction rates of different material areas are not uniform. This leads to non-uniform deformation along the tracks and between layers. The non-uniform contraction means that residual stress and deformations are dependent on the direction of scanning.

One of the first studies of residual stress in L-PBF was carried out by Shiomi et al. (2004) where the highest value of tensile residual stress was found at the top layer of the L-PBF part. Gusarov, Pavlov and Smurov (2011) showed that tensile stresses in AM depend on the shape of single tracks and maximum tensile stresses are two times greater in the longitudinal direction than in the transversal direction. Residual stress can be redistributed by the formation of cracks and pores, making the understanding of stress distribution even more complex. Yadroitsev and Yadroitsava (2015) studied residual stress in SS 316L and Ti6Al4V alloys and the residual stress on the top surface of the L-PBF objects were shown to be tensile and the maximum stress was in the scanning direction for all specimens.

Simson et al. (2017) showed the dependence of residual stress on the selected process parameters; the value and orientation of the main stress component depended on the analyzed layer of 316L steel. On the top surface, higher residual stress values were also found in the scan direction. The lateral surface revealed the highest main stress component was parallel to the building direction. These findings support the processes described by the temperature gradient mechanism and cool-down phase model (Figure 9.6). This study also showed that residual stress values depend on structural density. Figure 9.7a illustrates FEA simulations of the stress of rectangular Ti6Al4V solid blocks, fixed to the base plate, with initially high residual stress. Higher stresses are found at the bottom, where samples are attached to the base plate. If samples are separated from the base plate during processing, the sample deforms and the residual stress changes from the original configuration. Overhanging parts that have no direct metallurgical contact with the base plate are deformed during processing, thereby redistributing stress significantly (Figure 9.7b-e).

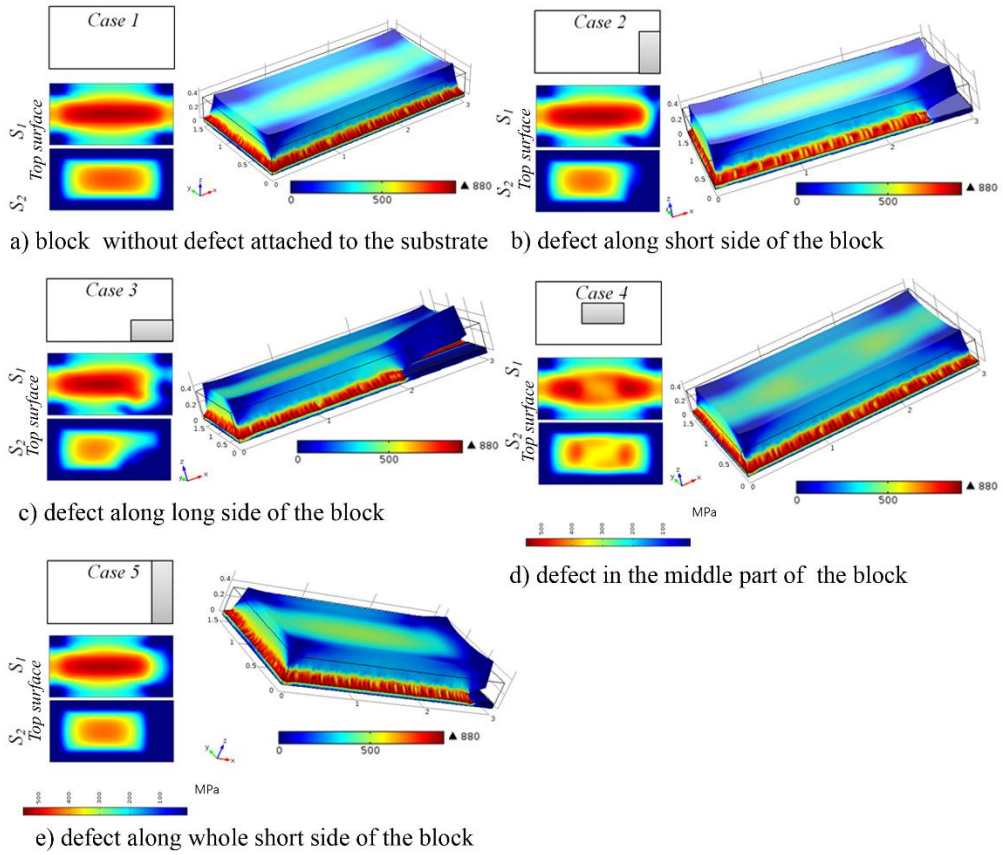

Figure 9.7. Residual stress in rectangular Ti6Al4V attached to base plate solid blocks (a) and blocks with defects – planar regions causing loss of attachment to the baseplate 0.005 mm^3 in size (b–e). Dimensions of the block are 3×1.5×0.3 mm (x, y, z), initial stress of solid block are σxx = 600 MPa, σyy = 900 MPa, σxy = σxz = 25 MPa. Scale factor for the deformation is 50 (van Zyl, Yadroitsava and Yadroitsev, 2016).

Numerical simulations have shown that residual stress is geometrically dependent on object shapes as well as building and scanning strategies applied (Nadammal et al., 2017; Parry, Ashcroft and Wildman, 2019). Parry, Ashcroft and Wildman (2019) showed that longitudinal stresses (along the scanning direction) have a threshold depending on scan length: it increases linearly up to a critical length of scanning, then they are almost constant. Transverse stresses were more sensitive to the thermal history than longitudinal ones.

Experiments with different shapes of samples were performed in Yadroitsava et al. (Yadroitsava *et al.*, 2015). Surface residual stress in Ti6Al4V objects of simple geometries (Figure 9.8) were measured by X-ray diffraction (XRD). Samples were scanned in a stripe pattern in back-and-forth directions with an EOSINT M280 system. For the semi-sphere without supports, the principal residual stress was lower in comparison with the inverted semi-sphere with supports. In prisms, the maximum residual stress near the top surface was

915 MPa, where the ratio of the top area to the base surface was 100:9. A prism with a lower ratio (100:36) had a lower residual stress of 628 MPa. It is possible that overheating led to higher values of residual stress for a prism with a small cross-section at the bottom, since local overheating is responsible for higher residual stress (Parry, Ashcroft and Wildman, 2019).

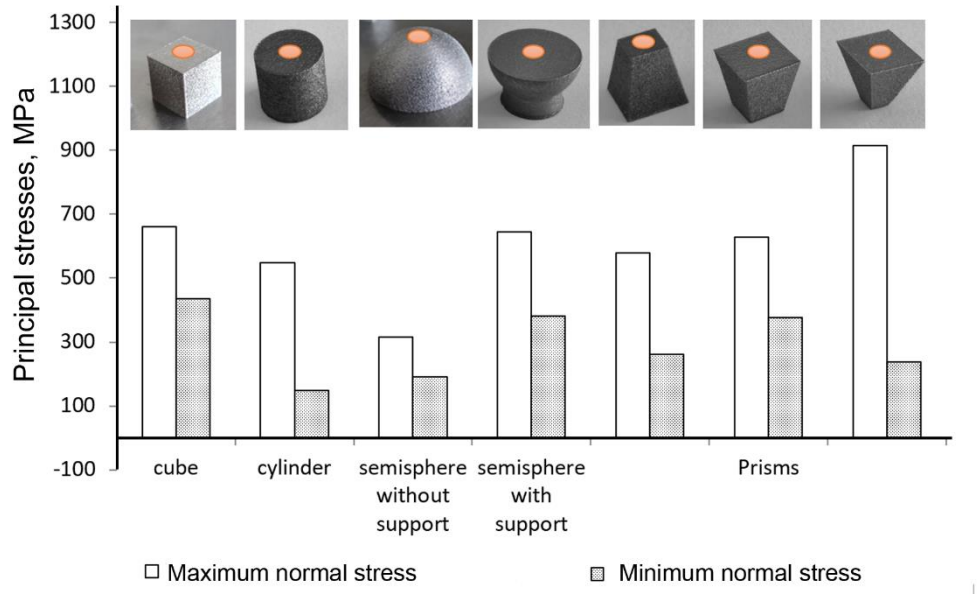

Figure 9.8. Principal stresses near the surface in 3D L-PBF Ti6Al4V objects attached to the substrate: cubes 10×10×10 mm^3 without support; cylinder with diameter 10 mm and height 10 mm; semi-spheres without/with supports, diameter 10 mm; prisms: height 10 mm, bottom base 10×10 mm^2, top base 6×6 mm^2; height 10 mm, bottom base 6×6 mm^2 and top base 10×10 mm^2; height 10 mm, bottom base 3×3 mm^2 and top base 10×10 mm^2. Orange points indicate where residual stress was measured.

Salmi et al. (2017) showed that in general, samples with supports had higher stress than specimens with direct contact with the base plate, mainly due to the different heat transmission modes along the building direction; thus, the thermal gradient was lower for samples without supports. Also, it was found that residual stress exhibited varying (oscillating) behavior with depth (Figure 9.9a). These variations indicate the non-uniform heat distribution and transfer, and a possible effect of microstructural changes on residual stress distribution. Previously, similar oscillating behavior of residual stress with depth in L-PBF samples was shown in (Yadroitsev and Yadroitsava, 2015), Figure 9.9b. Roughness has an influence on the residual stress value, as can be seen in Figure 9.9b. In SS 316L samples, residual stress was measured at the center near the surface: residual stress was relatively low for the first approximately 100 μm. This correlates with as-built roughness on the top surface that was 70 ± 20 μm. Electrolytic removal of layers was done to measure normal stresses in-depth by XRD.

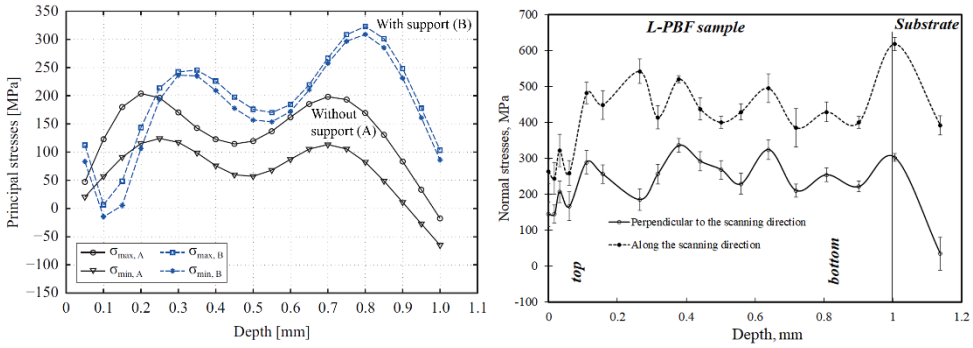

Figure 9.9. (a) Principal stresses in AlSi10Mg parallelepiped 30 × 20 × 10 mm³ samples manufactured with stripes scanning strategy with rotation of scanning direction in each layer of 67 degrees; the layer thickness is 30 μm, (Salmi *et al.*, 2017) **and a profile of the residual stress in cuboid 30×30×1 mm³ SS 316L sample (50 μm layer thickness) produced in one scanning direction that did not change during the manufacturing process (b), based on data from** (Yadroitsev and Yadroitsava, 2015)**.**

Cao et al. (2020) built inclined samples at angles (45, 60 and 75° to the horizontal) with and without supports from MS1 steel. It was found that samples without supports had slightly lower residual stress, but in these samples, residual stress was more unevenly distributed on the supporting surface. Generally, support structures act as heat sinks, hindering the conduction of heat away from the object under build, and leading to higher thermal stresses than when no supports are used.

Bayerlein et al. (2018) studied residual stress by performing neutron diffraction measurements for simple cuboid forms of Inconel 718 at different stages of the build-up (i.e. after one 20 μm-layer; at build heights of 4 mm and 20 mm; and for a fully built-up cuboid of 40 mm in height). High compressive and tensile stresses in three normal directions were found at the edges and around the middle part of the samples. Along the build direction, the stresses generally changed smoothly from tensile near the top surface to compressive stresses closer to the base plate. In addition, it should be noted that at later stages tensile stresses developed along the edges.

The distribution of residual stress is not straightforward and depends on many process conditions and object's shape. Zhao et al. (2020) found tensile stress near the base plate in as-built L-PBF Ti6Al4V and AlSi10Mg blocks (X×Y×Z of 150 mm × 5 mm ×35 mm built along the Z direction). These blocks, manufactured with reticulated support, also exhibited compressive stress in the middle section and tensile stress at the top section.

Brown et al. (2016) showed differences in residual stress distribution and magnitudes in L-PBF 17-4 steel Charpy samples using neutron diffraction measurements before and after separation from the base plate (Figure 9.10). It was found that the value of the residual stress was about two thirds of the yield

strength of the material. The largest residual stress in as-built samples was in the longitudinal direction (Fig. 9.10a and b). Sample A and C were built with similar process parameters, but sample A was suddenly separated from the support structure during processing (indicated as "Tear" in Figure 9.10a, d and f). The resulting asymmetric stress fields were found not only in the as-built sample A attached to the substrate, but also in a separated sample as opposed to a sample C that was manufactured without any defects.

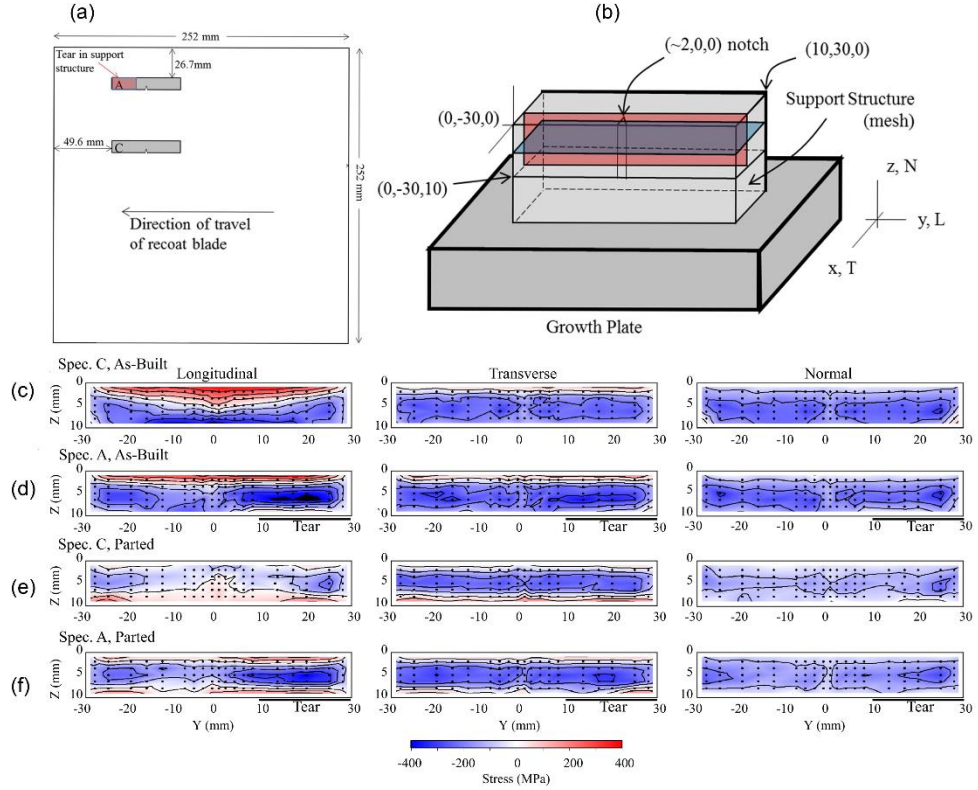

Figure 9.10. (a), (b) Schematic of build of Charpy specimens; (c) and (d) contour plots of longitudinal, transverse, and normal direction stresses, respectively, on an y-z plane (at x= 3.8 mm) in sample C and A, respectively, while still attached to support and base plate; (e) and (f): similar contour plots after removal from support and base plate., modified from Brown et al. (2016).

9.4. MODELING OF L-PBF PROCESS AND RESIDUAL STRESS EVOLUTION

Process modeling and monitoring plays an important role in detecting or predicting errors during AM. Modeling the L-PBF process from powder delivery, energy absorption, melting, solidification and cooling of the melt material up to the initiation of residual stress and evolution of different microstructure is a challenge. Many factors must be considered: the absorption of laser radiation and melting of powder material with randomly distributed

particles; thermal properties of the powder, liquid, and solid material; material properties at different temperatures; thermal gradient and cooling rates; microstructural and stress evolution; melt pool size and geometry, etc. (King et al., 2015; Khairallah et al., 2016). These phenomena define the resulting porosity, microstructure, the heat-affected-zone and stresses in L-PBF parts. The challenge with microscale models is the effort required, cost and long computational time. As indicated by Debroy et al. (2018), residual stress in AM is highly variable in spatial and temporal domains, so high-quality experimental data and accurate numerical simulation is required.

Melt pool geometry and temperature monitoring and control are essential in managing residual stress in situ. Unfortunately, it is difficult to execute experimental measurements of temperature during L-PBF (Krauss, Eschey and Zaeh, 2012; Li and Gu, 2014), Chapter 11. Limitations of the resolution, lengthy image processing and cost implications render monitoring of the melt pool very complex. Despite these challenges, machine learning is increasingly being used to study the vast data that can be gathered from camera-based melt pool monitoring.

It is often convenient to simulate the behavior of manufacturing processes under various conditions, rather than conduct experiments that could be prohibitively expensive. Finite Element Analysis (FEA) is commonly used to predict residual stress and distortions during L-PBF. FEA makes use of mathematical models that incorporate laws of physics and boundary conditions such as material properties to study how processes respond to a set of parameters. In L-PBF, 3D finite element modeling is currently widely used, although 2D elements still find useful applications in residual stress prediction. Wu et al. (2017) used a 2D thermo-mechanical model to study the melt pool and residual stress characteristics of AlSi10Mg parts by means of FEA and experimental evaluation using X-ray diffraction. Their simulation and experimental results coincided with experimental results showing compressive stress at the sample's mid-section and tensile stress at the edges.

Luo et al. (2018) introduced a 3D transient thermo-mechanically coupled finite element model to analyze the temperature and stress fields during L-PBF of SnTe. The predicted and experimental results showed concentration of thermal stress at the ends of the tracks and edges of the formed surface. Y. Li et al. (Y. Li *et al.*, 2018) showed with 3D thermal-mechanical modeling that the residual stress component in the building direction increases with the numbers of sintered layers. Lu et al. (2019) combined computer vision and FEM to estimate the stress development within a layer from melt and solid state surface displacement information.

Since L-PBF typically uses thin material layers, microscale modeling requires highly refined meshes. Researchers can overcome this challenge by simultaneously modeling a group of layers (Afazov et al., 2017).

Moser et al. (2019) developed a continuum thermo-mechanical model which approximates the powder as a continuous medium with effective material properties to avoid modeling powder particles individually. The results prove the viability of this approach for modeling residual stress. L-PBF specimens produced at similar process parameters can exhibit significant variation of measured residual stress (Georgilas, Khan and Kartal, 2020). This can be due to differences in specimen geometry, which can drastically change the heat transfer dynamics during manufacturing.

Developments in AM modeling have resulted in mesoscale modeling developed by Li et al. (2017), while Afavoz et al. (2017) developed an approach for modeling at the component scale. The results showed that distortion can be successfully compensated for in L-PBF parts inverting the distortions and incorporating them into the target geometry's CAD model.

Jayanath and Achuthan (2019) developed an FEA model which hybridizes the conventional FEA and inherent strain tensor-based models. Boruah et al. (2018) presented an experimentally-validated analytical model which can be used for prediction of residual stress distribution in L-PBF parts. The model is based on the force and moment equilibrium of induced stresses by progressive deposition of material layers. Researchers are also increasingly utilizing machine learning methods such as deep learning (Francis and Bian, 2019) to predict residual stress and distortions from thermal images and local heat transfer information. Recently, Bertini et al. (2019) analyzed simulation strategies in residual stress prediction during L-PBF. This review clearly indicates that at the present stage of L-PBF, meso-scale modeling is more widely applied in comparison with macro-scale simulations.

9.5. POST-PROCESSING STRESS RELIEVING

9.5.1. Heat treatment

It is a common practice in L-PBF to perform stress-relief heat treatment to relieve stresses that have built up during the process. Heat treatment is usually implemented before detaching parts from the base plate to avoid distortion upon separation (Manfredi et al., 2013; Pupo et al., 2013; Sames et al., 2016). Appropriate heat treatment relieves up to 70–90% of residual stress that is introduced by the L-PBF process (Shiomi *et al.*, 2004; Schneller *et al.*, 2019; Tong *et al.*, 2019). Kreitcberg et al. (2017) indicated that the stress-relieving heat treatment procedure has to be chosen carefully, because for some alloys it can lead to undesirable phenomena, such as carbide precipitation and phase changes, as happens in nickel alloys at 650-870°C stress-relieving temperature for example.

In some cases, despite the widespread use of heat treatment as a stress-relief technique, the process does not necessarily completely remove tensile residual stress. For example, Salmi et al. (2017) revealed the presence of high tensile stresses on the as-built AlSi10Mg L-PBF, despite performing stress-relieving thermal treatment. A special heat treatment procedure for L-PBF parts must be found and approved, since the structures have a specific microstructure that is different from that of materials obtained by traditional methods. Moreover, this microstructure depends on specific process parameters, scanning and building strategies which makes it challenging to find a generic solution (Chapters 12 and 13).

9.5.2. Mechanical treatment

Shot peening is the process of impacting the surface with high-speed shots (by metallic, ceramic or glass beads) to plastically deform the impacted surface and improve the fatigue performance. (Maamoun, Elbestawi and Veldhuis, 2018) showed that shot peening of AlSi10Mg samples decreased surface defects, refined microstructure and had a hardening effect while also introducing a relatively high compressive stress (–170 MPa) up to a 90-μm depth. This method was used also by Salmi and Atzeni (2017) for L-PBF AlSi10Mg samples after stress-relieving heat treatment. It was stated that a combination of optimal heat treatment with shot peening procedure will allow to introduce uniform compression stress into L-PBF samples.

Laser shock peening (LSP) can be applied in AM as a surface modification technique that alters the surface microstructure and mechanical properties (Guo et al., 2018). LSP is quite effective in reducing residual stress magnitudes, and even introducing desirable compressive stresses to the surface (Munther et al., 2020). Laser peening mimics the bulk deformation strengthening mechanisms such as rolling and shot peening. The effectiveness of LSP on surface modification and residual stress control depends on the selection of processing parameters such as laser energy, shot overlap, laser spot size, laser pulse duration, etc. (Kalentics *et al.*, 2017) used the hole drilling technique to investigate the effect of LSP parameters on surface residual stress. The value and depth of the compressive residual stress that was introduced was found to be dependent on the selected LSP parameters. In addition to the residual stress relief and compressive stress that is formed on the surface, the method was shown to close near-surface porosity in (du Plessis *et al.*, 2019), all of which contributes to improved fatigue properties. The cost of LSP prohibits the wide use of this stress-relieving method, but it can be applied to localized high stress areas for critical applications in aerospace, power generation and nuclear industries (Hackel et al., 2018).

The surface morphology of L-PBF parts is complex because it depends on many factors like powder size and particle shape, material, process parameters, scanning strategies, part orientation, etc. Industrial applications require high surface quality to prevent premature failure of the component that might arise from the initiation of cracks during use. Thus, many L-PBF parts inevitably demand ***machining***, and these machining operations also alter the stress state of the components. For example, surface tensile stress and a subsurface compressive stress induced by the milling operation were observed in L-PBF AlSi10Mg parts (Piscopo et al., 2019). In the research done by Sarkar et al. (2019), about –300 MPa compressive residual stress was found on the machined surface of L-PBF manufactured 15-5PH specimens. The compressive stress and reduced surface roughness induced by machining both led to improved fatigue life.

Ultrasonic impact treatment (UIT), whereby high-frequency ultrasonic oscillations are applied to the component, is used to eliminate tensile stress as well as to introduce compressive stress, to correct deformations and improve fatigue strength of welded structures. UIT also known as high frequency mechanical impact. UIT was tested on L-PBF parts by Malaki and Ding (Malaki and Ding, 2015), Lesyk et al. (Lesyk *et al.*, 2019), and Walker et al. (Walker *et al.*, 2019). Lesyk et al. (2019) applied this technique on Inconel 718 turbine blade test parts manufactured by L-PBF. In that study, the tensile stress (+120 MPa) observed for the as-built condition was transformed into a compressive stress (about –430 MPa) after application of UIT. The surface roughness, microhardness, and near-surface porosity were also improved. Additionally, Walker et al. (2019) showed that UIT enhances the fatigue life of L-PBF-manufactured Ti6Al4V parts by 200%, while significantly improving the surface integrity and introducing compressive stress into the components. Zhang et al. (2016) showed that the application of UIT during L-PBF reduces defects and residual stress, and obtains fine equi-axed grains. However, ultrasound waves can lead to powder entrapment near edges, which leads to reduced accuracy and high defectiveness of the side surfaces of the final product. UIT-induced smoothness of the surface of the processed layer also leads to problems with powder delivery for the next layer.

Many of the post-process interventions for controlling residual stress are quite effective, but they are incapable of reversing stress-induced deformations. Furthermore, post-processing substantially increases both manufacturing time and cost (Jayanath and Achuthan, 2019).

9.6 IN SITU STRESS RELIEF

The most popular in situ stress relief method is in situ thermal gradient management, which includes preheating of the substrate or powder bed, modification of scanning strategies and process parameters, i.e. control of

temperature gradients and cooling rates. Another in situ stress relief method is in situ mechanical impact that introduces compressive stress (since L-PBF generates high tensile stresses) by LSP or machining during manufacturing, so called “hybrid AM”.

9.6.1 Base plate and build chamber preheating

Residual stress is a function of thermal gradients brought about by the huge temperature difference between the melt pool and the “cold” surrounding material, i.e. powder and substrate (Figure 9.6). Preheating reduces this temperature difference and thus reduces thermal stresses. A study conducted by Shiomi et al. (2004) on chrome molybdenum steel demonstrated a 40% reduction of residual stress with the application of base plate preheating. Kempen et al. (2013) applied base plate preheating during the manufacturing of parts from M2 medium alloyed steel and managed to progressively reduce stress-induced cracking and delamination. Furumoto et al. (2010) achieved 80% residual stress reduction for an in situ alloyed mixture of chromium molybdenum steel, copper and nickel alloys by preheating the base plate. Reduction in residual stress was also reported in the work done by Kemerling et al. (2018) with 304L stainless steel after raising the preheating temperature to 250°C. It was shown that *Z*-directional stresses are a function of the preheating temperature. Mertens et al. (Mertens *et al.*, 2018) demonstrated that the effect of base plate preheating on residual stress and the stress-induced cracking does not follow the same trend for different materials (aluminum 7075 alloy, nickel alloy Hastelloy X, H13 tool steel and cobalt-chrome).

Zhang et al. (2013) implemented powder bed preheating up to 150 °C to prevent deformation and to improve the dimensional accuracy of 316L stainless steel tensile test specimens. The effectiveness of powder preheating on residual stress was demonstrated by Roberts (2012) who achieved up to 50% residual stress reduction in Ti6Al4V specimens by increasing the powder bed temperature from 40°C to 300 °C. In another study, Ali et al. (2017) reported a reduction of residual stress from 214 MPa to 1 MPa by raising the powder bed temperature from 100°C to 570 °C for Ti6Al4V.

A study by Malý et al. (2019) revealed the possibility of increased oxidation and particle agglomeration as a result of powder preheating. These findings clearly indicate that when preheated to high temperatures, powder reuse may not be suitable for the manufacture of mechanically strong parts, since higher oxygen and nitrogen contents are known to promote embrittlement in Ti6Al4V alloy and could lead to part failure (Tal-Gutelmacher and Eliezer, 2005; Yan et al., 2014).

It must be noted that powder preheating can be achieved by keeping the build chamber at an elevated temperature, but this temperature must be lower than the powder sintering temperature, since it influences the L-PBF process

(Yadroitsev et al., 2013). Preheating either the base plate or powder bed does not only affect the stress state of materials, but can also influence the achievable density (Mertens et al., 2018), microstructure (Yadroitsev et al., 2013; W. Li et al., 2016; Mertens et al., 2018) and mechanical properties (W. Li et al., 2016). An important aspect is the presence of a module for pre-heating chamber/base plate with high temperatures in commercial L-PBF systems. Such solutions require special optics, materials, special machine design, special safety measures, etc. Basically, all studies with the preheating of the substrate and powder are carried out in unique systems and experimental set-up.

9.6.2 Process parameter optimization

The effect of process parameters, such as laser power, layer thickness, scanning speed and hatch distance, on residual stress in L-PBF parts has been studied in Levkulich et al. (2019), Mugwagwa et al. (2018), and Vrancken et al. (2016). Levkulich et al. (2019) investigated the effect of laser power and scanning speed on residual stress in L-PBF Ti6Al4V parts by X-ray diffraction, hole drilling and contour methods. The results showed that residual stress near the surface decreased with increasing laser power and decreasing scanning speed: larger melt pools promote slower cooling rates and, therefore, lead to reductions in residual stress in metals. Thus, selecting high laser power and low scanning speeds can achieve residual stress reduction whilst maintaining acceptable part density.

However, a blanket adjustment of process parameters throughout the component's geometry may not be ideal. Depending on part geometry, parameters such as the scanning strategy may need to be adjusted from layer to layer (Meier and Haberland, 2008). Ali et al. (2019) established that residual stress can be managed by in situ temporary adjustment of the powder layer thickness. In their study, residual stress was reduced by 8.5% by increasing the layer thickness in areas with the predetermined high-stress zones for a given geometry. From another perspective, in order to produce non-porous parts with thicker layers, more energy must be introduced to re-melt the thicker powder layer and previously melted layer. The effect of layer thickness on residual stress was also investigated by measuring the deformation of bridge-shaped specimens (Kruth et al., 2012) and cantilever specimens (Zaeh and Branner, 2010; Mugwagwa et al., 2018). All these works indicate a decrease in deformation by increasing the layer thickness. Gao et al. (2018) also stated that increasing the layer thickness reduces the cooling rate and effectively lowers residual stress. Ali et al. (2018) showed that the decreased cooling rate of 40% caused by increasing the layer thickness from 25 μm to 75 μm was the primary reason for the reduction in deformation and residual stress. While increasing the layer thickness lowers residual stress, it was also shown that increasing the

layer thickness has a tendency to increase interlayer defects and percentage porosity, thereby compromising the mechanical properties (Ali, Ghadbeigi and Mumtaz, 2018; du Plessis, 2019).

In summary, there must be a reasonable "compromise" between reducing residual stress by increasing/decreasing power, scanning speed or hatch distance, or changing powder layer thickness or spot size, etc. to produce fully dense parts with the required accuracy, without cracks and distortions.

9.6.3. Scanning strategy and in situ residual stress control

Scanning strategies influence several process outcomes including residual stress, achievable density, microstructure and surface finish. Wang et al. (Wang *et al.*, 2018) indicated that a combination of scanning strategy and preheating temperature influence the residual stress direction, values and distribution; residual stress and grain microstructure are closely related thus influence on performance of L-PBF parts. Thermal stresses can be partially overcome by scanning strategy adjustment to improve uniformity of heating and shrinkage (Beal et al., 2008; Jhabvala et al., 2010).

One of the specific methods proposed to decrease thermal gradients is “chess board strategy”. This scanning strategy uses short scan tracks by dividing the scanning area into smaller randomly scanned subsections (usually 5 mm × 5 mm) (Yasa et al., 2009; Kruth et al., 2010, 2012; Carter et al., 2014) and is similar to the island scanning strategy. Kruth et al. (Kruth *et al.*, 2004) and Li et al. (2016), showed that the shorter scan track strategies yield lower stresses and distortions compared to strategies that employ longer tracks. However, Parry et al. (Parry, Ashcroft and Wildman, 2016) demonstrated the geometric effect of scanning strategies on the build-up of residual stress, with indications of overheating where scan tracks become excessively short. Song et al. (Song *et al.*, 2018) corroborated these results, both numerically and experimentally. Ganeriwala et al. (2019) measured residual stress with X-ray diffraction in Ti6Al4V bridges and revealed higher residual stress, especially near the boundaries of the bridges that were built using island strategies in comparison with parts built with continuous zig-zag scans. Chen et al. (2019) also studied the effect of overlap rate on residual stress in L-PBF of Ti6Al4V and it was observed that overlap rates of 25–50% between islands (by using the island scanning strategy) led to reduction of residual stress due to rescanning effects introduced during the overlap. However, with an increase in the overlap rate, there is an accompanying long scanning track and a weakened pre-heating effect on the next island, leading to higher thermal gradients and stresses. The paintbrush or stripe strategy was developed also with the aim of reducing thermal stresses by shortening the scan tracks. The common practice

resulting in more isotropic stress distribution is to rotate the scanning direction between successive layers (Kempen, 2015; C. Li, Guo, *et al.*, 2018).

Rescanning is an approach whereby the laser beam passes over the powder layer more than once. Most of the studies on rescanning adopt the same process parameters as those used to melt the powder in the first pass. Wei et al. (2019) investigated rescanning in L-PBF of a Ti-5Al-2.5Sn alloy. In that study, rescanning once did not yield any reduction in residual stress. In fact, rescanning induced an increase in the maximum principal stress from 478 ± 33 MPa to 562 ± 14 MPa. However, applying a second rescan lowered the maximum stress to 288 ± 47 MPa, representing a reduction of approximately 39%. In similar work on Ti6Al4V by Xiao et al. (2020), rescanning up to four times was done to study the effect of rescanning cycles on density and residual stress. It must be noted that the rescanning was done with process parameters similar to the powder processing. Small cuboid parts were manufactured with dimensions of 15 mm × 15 mm × 5 mm. Excessive heating resulted in slightly higher porosity of samples that were rescanned four times for each layer, but in general, all relative densities were near 99%. The residual stress in samples that were not rescanned was about 450 MPa. After one-cycle rescanning, it increased to about 620 MPa and then decreased on subsequent rescans, albeit non-uniformly, reaching approximately 400 MPa at the fourth rescan cycle. Effectively, this represents only about 11% stress reduction as a result of applying four rescans.

Shiomi et al. (2004) reported that rescanning every layer at the same process parameters reduced residual stress by up to 55%. Mercelis and Kruth (2006) observed a 30% residual stress reduction in 316L stainless steel parts when implementing rescanning at 50% of the initial pass laser power. The application of rescanning does not only lower residual stress and its effects, but also significantly reduces top surface roughness (Yu et al., 2019), refines/modifies the microstructure (Wei et al., 2019), and increases density (Yu *et al.*, 2019) of L-PBF manufactured parts. A major setback with rescanning is the increase in manufacturing time and possible structural changes in material subjected to multiple heating/cooling cycles. Obviously, this increase in manufacturing time is directly proportional to the actual number of rescanning treatments performed.

Instead of using single or dual lasers, multiple-beam laser systems are becoming available for use in L-PBF. The multiple-beam strategies are a promising instrument for residual stress reduction during L-PBF processing, since multiple laser passes promote more uniform temperature distribution and reduce the cooling speeds within and around the melt pool (Heeling and Wegener, 2018). This can ultimately reduce thermal gradients and the associated stresses. Roehling et al. (2019) utilized multiple diodes to homogeneously illuminate the surface of the manufactured part, yielding a

90% reduction of residual stress magnitude. Their study also revealed that meaningful reduction in residual stress is only achievable when the diode power density generates sufficiently high temperature – called critical temperature – to achieve the annealing (in this case approximately 625 °C, attained using 840 W diode power).

However, any scanning strategy adjustment must take into consideration the part geometry that is being processed. Scanning strategies that are suitable for wide areas (for example chessboard strategies) may not be applicable for the fabrication of thin walls. (Meier and Haberland, 2008) pointed out that scanning strategies should be optimized for different geometries, and that they should even be altered layer by layer in order to accommodate changes in the geometry. The 3-axis scanning systems in modern L-PBF machines allow manipulation of the scanning strategy parameters for every layer as needed. For example, it is possible to change the scanning strategy as well as the laser power, scanning speed and spot size for a specific layer.

9.6.4. Optimization of support structures

During the manufacture of overhanging features, support structures are usually required. Designs and orientations that minimize the volume of supports are preferred as they reduce residual stress magnitudes (Cheng and To, 2019). Töppel et al. (2016) showed that the type of support structure influences both heat dissipation and residual stress.

L-PBF has enabled freedom of design such that certain topological features of components can be optimized to not only reduce weight, but to enhance product performance through avoiding residual stress in pre-processing. On the one hand, optimization of support structures is used to avoid overheating; on the other hand, to prevent deformation of manufactured parts. Engineers can now design against distortion by utilizing the strengths of topology optimization and modeling. Allaire and Bogosel (2018) presented mathematical models in which supports were optimized to improve the stiffness of the supported structure as well as cooling during manufacturing. Cheng et al. (2019) used the topology optimization technique to design support structures with the aim of preventing residual stress-induced failure. The optimized lattice support structure resulted in approximately 70% less stress-induced distortion compared to uniform lattice and toothed supports.

9.6.5. Optimization of alloy composition

Microcracking in L-PBF requires special attention. Xu et al. (2020) recently studied L-PBF of 2xxx series Al–Cu–Mg–Li–Zr alloys and showed that cracks developed during cooling were linked with specific microstructure that was

composed of long columnar grains. High cooling and solidification rates lead to high stress perpendicular to dendritic structure and hot cracking occurs.

The probability of solidification cracks increases with the range of solidification temperature of alloys because it is directly linked with solidification strain. To prevent the formation and propagation of hot cracks, modification in the chemical composition of the alloy by the addition of special elements that increase ductility and tensile strength in the solidification range as well as fine microstructure was used by Montero Sistiaga et al. (2016), Wang et al. (2019), and Xu et al. (2020).

To increase thermal shock resistance of AM nickel alloys, Harrison et al. (2015) proposed a minority increase in concentration of substitutional solid-solution-strengthening atoms within the lattice that increases ultimate tensile strength and yield stress at elevated temperature, thereby suppressing crack formation. Thus, there is need for the development of special alloys that take into account the specifics of high temperature gradients, cooling rates and solidification as well as internal stresses for L-PBF.

9.7 CONCLUSIONS

Recently, Schmeiser et al. (2020) studied stress formation in L-PBF by in situ X-ray diffraction. It was found that stress states in L-PBF specimens changed continuously up until the last laser beam exposure. Thus, different materials, process parameters and building strategies, as well as geometry, are influencing factors on spatial distribution and values of residual stress in L-PBF objects. Analysis of studies in the field of residual stresses shows the multidirectional research and the lack of a unified approach. Outstanding capabilities of LPBF allow working not only with different materials, but also with different shapes and sizes of parts produced with different systems, which significantly complicates the task. L-PBF parts are produced with different process parameters, scanning strategies and environmental parameters, etc. For investigations, substrates with different geometries and initial stresses are used, as well as various support structures for parts. Comprehensive reviews on residual stress modeling and control and its effects on performance of L-PBF parts can be found in (Bartlett and Li, 2019; Azarmi and Sevostianov, 2020; Fang *et al.*, 2020) etc. Control of residual stress cannot be separated from the study of material properties, which have been shown to be closely related to the L-PBF microstructure (C. Li, Liu, et al., 2018) and porosity (Mugwagwa et al., 2018; Georgilas, Khan and Kartal, 2020).

Residual stress in L-PBF is a result of non-uniform cooling and solidification and steep thermal gradients. Three main methods for residual stress control are evident – these are pre-process, in situ and post-processing techniques. Pre-process methods include careful process parameter selection and optimization as well as predictive and corrective numerical modeling. During the process

planning stage, it is vital to understand the thermo-mechanical behavior of the material being processed. The major in situ methods of managing residual stress are process parameter adjustment, scanning strategy optimization, feedback control and preheating. Post-processing methods are either thermal (heat treatment) or mechanical (peening, machining, etc.) processing.

In this chapter, the residual stress arising in L-PBF, the reasons for its occurrence and the methods for reducing it were presented. The choice of residual stress relief techniques does not only influence the final stress state of end products but also significantly affects manufacturing viability with regard to time and cost. The following conclusions can be made:

- Process parameters, such as laser power, scanning speed, layer thickness, preheating, scanning strategies, material and geometry of the object have an influence on the melt pool geometry, cooling rates and thermal gradients, as well as the resulting residual stress in L-PBF parts. Further analysis of the relationship between residual stress and these factors, as well as new materials developed specifically for L-PBF, are required.
- L-PBF is a complex thermal process, and, therefore, in situ monitoring and control is necessary. Melt pool monitoring and temperature measurements during L-PBF generate big data that can be used for machine-learning-based residual stress control. However, it is also beneficial to couple process monitoring with feedback control in order to implement corrective action in situ.
- Numerical modeling for the prediction of residual stress remains a powerful tool during the process planning stage where suitable process parameters and scanning strategy can be selected based on predicted behavior of L-PBF parts during manufacturing.
- Control over homogeneity of heating and cooling is critical in managing residual stress. Careful selection and adjustment of scanning strategies can achieve uniform solidification and heat distribution, thereby reducing residual stress. Additionally, managing cooling rates is a major step towards residual stress control. Both scanning strategies and process parameters can be manipulated to achieve this.
- Currently, the most used residual stress management approach so far lies in base plate preheating and post-process heat treatment. Although powder preheating has been reported, limited studies have been performed on how this could affect surrounding powder.
- New approaches, such as exposing a processed layer to intense light and heat (rather than rescanning), have the potential to unlock new ways of in situ residual stress control. The use of laser diodes for this purpose has commenced.

QUESTIONS

- What is residual stress?
- How can residual stress in a polycrystalline material be categorized according to length scales?
- What methods of residual stress measurement exist? Explain main principles of these methods.
- How does residual stress influence mechanical properties of components?
- What defects are associated with residual stress in L-PBF?
- Explain the origin of residual stresses during L-PBF.
- Explain the development of residual stress in L-PBF in terms of heating/cooling cycles.
- Why does residual stress depend on process parameters?
- Why does residual stress depend on scanning strategy?
- How do support structures affect the development of residual stresses in L-PBF?
- How can one decrease/remove the residual stress in-situ?
- Why is preheating an effective method for reducing residual stresses?
- What mechanical methods exist to relieve residual stress in L-PBF parts?

REFERENCES

Acevedo, R. *et al.* (2020) "Residual stress analysis of additive manufacturing of metallic parts using ultrasonic waves: State of the art review," *Journal of Materials Research and Technology*, 9(7), pp. 9457–9477. doi: https://doi.org/10.1016/j.jmrt.2020.05.092.

Afazov, S. *et al.* (2017) "Distortion prediction and compensation in selective laser melting," *Additive Manufacturing*. Elsevier B.V., 17, pp. 15–22. doi: 10.1016/j.addma.2017.07.005.

Ahmad, B. *et al.* (2018) "Residual stress evaluation in selective-laser-melting additively manufactured titanium (Ti-6Al-4V) and inconel 718 using the contour method and numerical simulation," *Additive Manufacturing*. Elsevier B.V., 22, pp. 571–582. doi: 10.1016/j.addma.2018.06.002.

Ali, H. *et al.* (2017) "In-situ residual stress reduction, martensitic decomposition and mechanical properties enhancement through high temperature powder bed pre-heating of selective laser melted Ti6Al4V," *Materials Science and Engineering A*, 695, pp. 211–220. doi: 10.1016/j.msea.2017.04.033.

Ali, H. *et al.* (2019) "Effect of pre-emptive in situ parameter modification on residual stress distributions within selective laser-melted Ti6Al4V components," *The International Journal of Advanced Manufacturing Technology*. The International Journal of Advanced Manufacturing Technology, 103(9–12), pp. 4467–4479. doi: 10.1007/s00170-019-03860-6.

Ali, H., Ghadbeigi, H. and Mumtaz, K. (2018) "Processing parameter effects on

residual stress and mechanical properties of selective laser melted Ti6Al4V," *Journal of Materials Engineering and Performance*. Springer US, 27(8), pp. 4059–4068. doi: 10.1007/s11665-018-3477-5.

Allaire, G. and Bogosel, B. (2018) "Optimizing supports for additive manufacturing," *Structural and Multidisciplinary Optimization*, 58(6), pp. 2493–2515. doi: 10.1007/s00158-018-2125-x.

Azarmi, F. and Sevostianov, I. (2020) "Evaluation of the residual stresses in metallic materials produced by additive manufacturing technology: effect of microstructure," *Current Opinion in Chemical Engineering*. Elsevier Ltd, pp. 21–27. doi: 10.1016/j.coche.2019.12.004.

Bartlett, J. L. and Li, X. (2019) "An overview of residual stresses in metal powder bed fusion," *Additive Manufacturing*. Elsevier B.V., pp. 131–149. doi: 10.1016/j.addma.2019.02.020.

Bayerlein, F. *et al.* (2018) "Transient development of residual stresses in laser beam melting – A neutron diffraction study," *Additive Manufacturing*. Elsevier, 24(March 2017), pp. 587–594. doi: 10.1016/j.addma.2018.10.024.

Beal, V. E. *et al.* (2008) "Scanning strategies and spacing effect on laser fusion of H13 tool steel powder using high power Nd:YAG pulsed laser," *International Journal of Production Research*, 46(1), pp. 217–232. doi: 10.1080/00207540500168279.

Bertini, L. *et al.* (2019) "Residual stress prediction in selective laser melting: A critical review of simulation strategies," *International Journal of Advanced Manufacturing Technology*. Springer London, 105(1–4), pp. 609–636. doi: 10.1007/s00170-019-04091-5.

Boruah, D., Zhang, X. and Doré, M. (2018) "An analytical method for predicting residual stress distribution in selective laser melted/sintered alloys," in *Materials Research Proceedings*. Leuven: Materials Research Form LLC, pp. 283–288. doi: 10.21741/9781945291890-45.

Brown, D. W. *et al.* (2016) "Neutron diffraction measurements of residual stress in additively manufactured stainless steel," *Materials Science and Engineering A*. Elsevier Ltd, 678, pp. 291–298. doi: 10.1016/j.msea.2016.09.086.

Buchbinder, D. *et al.* (2014) "Investigation on reducing distortion by preheating during manufacture of aluminum components using selective laser melting," *Journal of Laser Applications*. Laser Institute of America, 26(1), p. 012004. doi: 10.2351/1.4828755.

Cao, Q. *et al.* (2020) "The effect of support structures on maraging steel MS1 parts fabricated by selective laser melting at different building angles," *Rapid Prototyping Journal*. Emerald Group Publishing Ltd. doi: 10.1108/RPJ-11-2019-0287.

Carter, L. N. *et al.* (2014) "The influence of the laser scan strategy on grain structure and cracking behaviour in SLM powder-bed fabricated nickel superalloy," *Journal of Alloys and Compounds*, 615, pp. 338–347. doi: 10.1016/j.jallcom.2014.06.172.

Chen, C. *et al.* (2019) "Effect of overlap rate and pattern on residual stress in selective laser melting," *International Journal of Machine Tools and Manufacture*. Elsevier

Ltd, 145(December 2018), p. 103433. doi: 10.1016/j.ijmachtools.2019.103433.

Cheng, L. *et al.* (2019) "On utilizing topology optimization to design support structure to prevent residual stress induced build failure in laser powder bed metal additive manufacturing," *Additive Manufacturing*. Elsevier, 27(February), pp. 290–304. doi: 10.1016/j.addma.2019.03.001.

Cheng, L. and To, A. (2019) "Part-scale build orientation optimization for minimizing residual stress and support volume for metal additive manufacturing: Theory and experimental validation," *CAD Computer Aided Design*. Elsevier Ltd, 113, pp. 1–23. doi: 10.1016/j.cad.2019.03.004.

Cruz, V. *et al.* (2020) "Electrochemical studies on the effect of residual stress on the corrosion of 316L manufactured by selective laser melting," *Corrosion Science*. Elsevier Ltd, 164, p. 108314. doi: 10.1016/j.corsci.2019.108314.

DebRoy, T. *et al.* (2018) "Additive manufacturing of metallic components – Process, structure and properties," *Progress in Materials Science*. Elsevier Ltd, pp. 112–224. doi: 10.1016/j.pmatsci.2017.10.001.

Fang, Z. C. *et al.* (2020) "Review on residual stress in selective laser melting additive manufacturing of alloy parts," *Optics and Laser Technology*. Elsevier Ltd, p. 106283. doi: 10.1016/j.optlastec.2020.106283.

Francis, J. and Bian, L. (2019) "Deep learning for distortion prediction in laser-based additive manufacturing using big data," *Manufacturing Letters*. Society of Manufacturing Engineers (SME), 20, pp. 10–14. doi: 10.1016/j.mfglet.2019.02.001.

Furumoto, T. *et al.* (2010) "Study on reduction of residual stress induced during rapid tooling process: Influence of heating conditions on residual Stress," *Key Engineering Materials*, 447–448, pp. 785–789. doi: 10.4028/www.scientific.net/KEM.447-448.785.

Ganeriwala, R. K. *et al.* (2019) "Evaluation of a thermomechanical model for prediction of residual stress during laser powder bed fusion of Ti-6Al-4V," *Additive Manufacturing*. Elsevier B.V., 27, pp. 489–502. doi: 10.1016/j.addma.2019.03.034.

Gao, P. *et al.* (2018) "Influence of layer thickness on microstructure and mechanical properties of selective laser melted Ti-5Al-2.5Sn alloy," *Jinshu Xuebao/Acta Metallurgica Sinica*, 54(7), pp. 999–1009. doi: 10.11900/0412.1961.2017.00384.

Georgilas, K., Khan, R. H. U. and Kartal, M. E. (2020) "The influence of pulsed laser powder bed fusion process parameters on Inconel 718 material properties," *Materials Science and Engineering A*. Elsevier B.V., 769(June 2019), p. 138527. doi: 10.1016/j.msea.2019.138527.

Guo, W. *et al.* (2018) "Laser shock peening of laser additive manufactured Ti6Al4V titanium alloy," *Surface and Coatings Technology*, 349(February), pp. 503–510. doi: 10.1016/j.surfcoat.2018.06.020.

Gusarov, A. V., Pavlov, M. and Smurov, I. (2011) "Residual stresses at laser surface remelting and additive manufacturing," *Physics Procedia*, 12(PART 1), pp. 248–254. doi: 10.1016/j.phpro.2011.03.032.

Hackel, L. *et al.* (2018) “Laser peening: A tool for additive manufacturing post-processing,” *Additive Manufacturing*. Elsevier B.V., 24, pp. 67–75. doi: 10.1016/j.addma.2018.09.013.

Harrison, N. J., Todd, I. and Mumtaz, K. (2015) “Reduction of micro-cracking in nickel superalloys processed by Selective Laser Melting: A fundamental alloy design approach,” *Acta Materialia*. Elsevier Ltd, 94, pp. 59–68. doi: 10.1016/j.actamat.2015.04.035.

Heeling, T. and Wegener, K. (2018) “The effect of multi-beam strategies on selective laser melting of stainless steel 316L,” *Additive Manufacturing*. Elsevier, 22, pp. 334–342. doi: 10.1016/j.addma.2018.05.026.

Jayanath, S. and Achuthan, A. (2019) “A computationally efficient hybrid model for simulating the additive manufacturing process of metals,” *International Journal of Mechanical Sciences*. Elsevier Ltd, 160(February), pp. 255–269. doi: 10.1016/j.ijmecsci.2019.06.007.

Jhabvala, J. *et al.* (2010) “On the effect of scanning strategies in the selective laser melting process,” *Virtual and Physical Prototyping*, 5(2), pp. 99–109. doi: 10.1080/17452751003688368.

Kalentics, N. *et al.* (2017) “Tailoring residual stress profile of selective laser melted parts by laser shock peening,” *Additive Manufacturing*, 16, pp. 90–97. doi: 10.1016/j.addma.2017.05.008.

Kemerling, B. *et al.* (2018) “Residual stress evaluation of components produced via direct metal laser sintering,” *Welding in the World*, 62(3), pp. 663–674. doi: 10.1007/s40194-018-0572-z.

Kempen, K. *et al.* (2013) “Lowering thermal gradients in selective laser melting by pre-heating the baseplate,” in *Solid Freeform Fabrication Symposium*. Austin.

Kempen, K. (2015) *Expanding the materials palette for selective laser melting of metals*. PhD Thesis, KU Leuven.

Khairallah, S. A. *et al.* (2016) “Laser powder-bed fusion additive manufacturing: Physics of complex melt flow and formation mechanisms of pores, spatter, and denudation zones,” *Acta Materialia*. Elsevier Ltd, 108, pp. 36–45. doi: 10.1016/j.actamat.2016.02.014.

King, W. E. *et al.* (2015) “Laser powder bed fusion additive manufacturing of metals; physics, computational, and materials challenges,” *Applied Physics Reviews*, 2(4), p. 041304. doi: 10.1063/1.4937809.

Knowles, C., Becker, T. and Tait, R. (2012) “Residual stress measurements and structural integrity implications for selective laser melted Ti-6Al-4V,” *South African Journal of Industrial Engineering*, 23(3), pp. 119–129. doi: 10.7166/23-3-515.

Krauss, H., Eschey, C. and Zaeh, M. F. (2012) “Thermography for monitoring the selective laser melting process,” in *Solid Freeform Fabrication Symposium*. Austin, pp. 999–1014.

Kreitcberg, A., Brailovski, V. and Turenne, S. (2017) “Effect of heat treatment and

hot isostatic pressing on the microstructure and mechanical properties of Inconel 625 alloy processed by laser powder bed fusion," *Materials Science and Engineering A*. Elsevier B.V., 689(February), pp. 1–10. doi: 10.1016/j.msea.2017.02.038.

Kruth, J.-P. *et al.* (2012) "Assessing and comparing influencing factors of residual stresses in selective laser melting using a novel analysis method," *Proceedings of the Institution of Mechanical Engineers, Part B: Journal of Engineering Manufacture*, 226(6), pp. 980–991. doi: 10.1177/0954405412437085.

Kruth, J. *et al.* (2010) "Part and material properties in selective laser melting of metals," in *16th International Symposium on Electromachining*, pp. 1–12.

Kruth, J. P. *et al.* (2004) "Selective laser melting of iron-based powder," in *Journal of Materials Processing Technology*. Elsevier, pp. 616–622. doi: 10.1016/j.jmatprotec.2003.11.051.

Lesyk, D. A. *et al.* (2019) "Post-processing of the Inconel 718 alloy parts fabricated by selective laser melting: Effects of mechanical surface treatments on surface topography, porosity, hardness and residual stress," *Surface and Coatings Technology*. Elsevier, 381, p. 125136. doi: 10.1016/J.SURFCOAT.2019.125136.

Levkulich, N. C. *et al.* (2019) "The effect of process parameters on residual stress evolution and distortion in the laser powder bed fusion of Ti-6Al-4V," *Additive Manufacturing*. Elsevier, 28(May), pp. 475–484. doi: 10.1016/j.addma.2019.05.015.

Li, C. *et al.* (2016) "A multiscale modeling approach for fast prediction of part distortion in selective laser melting," *Journal of Materials Processing Technology*, 229, pp. 703–712. doi: 10.1016/j.jmatprotec.2015.10.022.

Li, C. *et al.* (2017) "Efficient predictive model of part distortion and residual stress in selective laser melting," *Additive Manufacturing*, 17, pp. 157–168. doi: 10.1016/j.addma.2017.08.014.

Li, C., Guo, Y., *et al.* (2018) "A scalable predictive model and validation for residual stress and distortion in selective laser melting," *CIRP Annals - Manufacturing Technology*, 67, pp. 249–252. doi: 10.1016/j.cirp.2018.04.105.

Li, C., Liu, Z. Y., *et al.* (2018) "Residual Stress in Metal Additive Manufacturing," *Procedia CIRP*, 71, pp. 348–353. doi: 10.1016/j.procir.2018.05.039.

Li, W. *et al.* (2016) "Effect of substrate preheating on the texture, phase and nanohardness of a Ti-45Al-2Cr-5Nb alloy processed by selective laser melting," *Scripta Materialia*. Elsevier Ltd, 118, pp. 13–18. doi: 10.1016/j.scriptamat.2016.02.022.

Li, Y. *et al.* (2018) "Modeling temperature and residual stress fields in selective laser melting," *International Journal of Mechanical Sciences*. Elsevier Ltd, 136, pp. 24–35. doi: 10.1016/j.ijmecsci.2017.12.001.

Li, Y. and Gu, D. (2014) "Thermal behavior during selective laser melting of commercially pure titanium powder: Numerical simulation and experimental study," *Additive Manufacturing*, 1–4, pp. 99–109. doi: 10.1016/j.addma.2014.09.001.

Liang, X. *et al.* (2020) "On Incorporating Scanning Strategy Effects into the Modified

Inherent Strain Modeling Framework for Laser Powder Bed Fusion," *Additive Manufacturing*. Elsevier BV, p. 101648. doi: 10.1016/j.addma.2020.101648.

Lord, J. D., Penn, D. and Whitehead, P. (2008) "The application of digital image correlation for measuring residual stress by incremental hole drilling," *Applied Mechanics and Materials*, 13–14, pp. 65–73. doi: 10.4028/www.scientific.net/AMM.13-14.65.

Lu, J. (2002) "Prestress engineering of structural material: A global design approach to the residual stress problem," in G.Totten , M.Howes, T. I. (ed.) *Handbook of residual stress and deformation of steel*. Ohio: ASM International, pp. 11–26.

Lu, Y. *et al.* (2019) "Online stress measurement during laser-aided metallic additive manufacturing," *Scientific Reports*, 9, p. 7630. doi: 10.1038/s41598-019-39849-0.

Luo, C. *et al.* (2018) "Finite element analysis of temperature and stress fields during the selective laser melting process of thermoelectric SnTe," *Journal of Materials Processing Technology*. Elsevier, 261, pp. 74–85. doi: 10.1016/j.jmatprotec.2018.06.001.

Maamoun, A., Elbestawi, M. and Veldhuis, S. (2018) "Influence of Shot Peening on AlSi10Mg Parts Fabricated by Additive Manufacturing," *Journal of Manufacturing and Materials Processing*. MDPI AG, 2(3), p. 40. doi: 10.3390/jmmp2030040.

Malaki, M. and Ding, H. (2015) "A review of ultrasonic peening treatment," *Materials and Design*. Elsevier Ltd, 87, pp. 1072–1086. doi: 10.1016/j.matdes.2015.08.102.

Malý, M. *et al.* (2019) "Effect of process parameters and high-temperature preheating on residual stress and relative density of Ti6Al4V processed by selective laser melting," *Materials*, 12, p. 930. doi: 10.3390/ma12060930.

Manfredi, D. *et al.* (2013) "From powders to dense metal parts: Characterization of a commercial AlSiMg alloy processed through direct metal laser sintering," *Materials*, 6(3), pp. 856–869. doi: 10.3390/ma6030856.

Meier, H. and Haberland, C. (2008) "Experimental studies on selective laser melting of metallic parts," *Materialwissenschaft und Werkstofftechnik*, 39(9), pp. 665–670. doi: 10.1002/mawe.200800327.

Mercelis, P. and Kruth, J. (2006) "Residual stresses in selective laser sintering and selective laser melting," *Rapid Prototyping Journal*, 12(5), pp. 254–265. doi: 10.1108/13552540610707013.

Mercelis, P. and Kruth, J. P. (2006) "Residual stresses in selective laser sintering and selective laser melting," *Rapid Prototyping Journal*, 12(5), pp. 254–265. doi: 10.1108/13552540610707013.

Mertens, R. *et al.* (2018) "Application of base plate preheating during selective laser melting," in *Procedia CIRP*. Elsevier B.V., pp. 5–11. doi: 10.1016/j.procir.2018.08.002.

Montero Sistiaga, M. L. *et al.* (2016) "Changing the alloy composition of Al7075 for better processability by selective laser melting," *Journal of Materials Processing Technology*. Elsevier Ltd, 238, pp. 437–445. doi: 10.1016/j.jmatprotec.2016.08.003.

Moser, D., Cullinan, M. and Murthy, J. (2019) "Multi-scale computational modeling of residual stress in selective laser melting with uncertainty quantification," *Additive Manufacturing*. Elsevier, 29(December 2018), p. 100770. doi: 10.1016/j.addma.2019.06.021.

Mugwagwa, L. *et al.* (2018) "Influence of process parameters on residual stress related distortions in selective laser melting," *Procedia Manufacturing*. Elsevier B.V., 21(2017), pp. 92–99. doi: 10.1016/j.promfg.2018.02.099.

Munther, M. *et al.* (2020) "Laser shock peening and its effects on microstructure and properties of additively manufactured metal alloys: a review," *Engineering Research Express*. IOP Publishing, 2(2), p. 022001. doi: 10.1088/2631-8695/ab9b16.

Nadammal, N. *et al.* (2017) "Effect of hatch length on the development of microstructure, texture and residual stresses in selective laser melted superalloy Inconel 718," *Materials and Design*. Elsevier Ltd, 134, pp. 139–150. doi: 10.1016/j.matdes.2017.08.049.

Neugebauer, F. *et al.* (2014) "Multi scale FEM simulation for distortion calculation in additive manufacturing of hardening stainless steel," in *International Workshop on Thermal forming and welding distortion*. Bremen, pp. 1–11.

Örnek, C. (2018) "Additive manufacturing–a general corrosion perspective," *Corrosion Engineering Science and Technology*. Taylor and Francis Ltd., 53(7), pp. 531–535. doi: 10.1080/1478422X.2018.1511327.

Pagliaro, P. *et al.* (2010) "Measuring multiple residual-stress components using the contour method and multiple cuts," *Experimental Mechanics*, 50(2), pp. 187–194. doi: 10.1007/s11340-009-9280-3.

Parry, L. A., Ashcroft, I. A. and Wildman, R. D. (2019) "Geometrical effects on residual stress in selective laser melting," *Additive Manufacturing*. Elsevier, 25(September 2018), pp. 166–175. doi: 10.1016/j.addma.2018.09.026.

Parry, L., Ashcroft, I. A. and Wildman, R. D. (2016) "Understanding the effect of laser scan strategy on residual stress in selective laser melting through thermo-mechanical simulation," *Additive Manufacturing*. Elsevier B.V., 12, pp. 1–15. doi: 10.1016/j.addma.2016.05.014.

Piscopo, G. *et al.* (2019) "Machining induced residual stresses in AlSi10Mg component produced by Laser Powder Bed Fusion (L-PBF)," *Procedia CIRP*. Elsevier B.V., 79, pp. 101–106. doi: 10.1016/j.procir.2019.02.019.

du Plessis, A. *et al.* (2018) "X-Ray Microcomputed Tomography in Additive Manufacturing: A Review of the Current Technology and Applications," *3D Printing and Additive Manufacturing*. Mary Ann Liebert Inc., 5(3), pp. 227–247. doi: 10.1089/3dp.2018.0060.

du Plessis, A. (2019) "Effects of process parameters on porosity in laser powder bed fusion revealed by X-ray tomography," *Additive Manufacturing*, 30, p. 100871. doi: 10.1016/j.addma.2019.100871.

du Plessis, A. *et al.* (2019) "Pore closure effect of laser shock peening of additively manufactured AlSi10Mg," *3D Printing and Additive Manufacturing*, 6(5), pp. 245–

252. doi: 10.1089/3dp.2019.0064.

Pupo, Y. *et al.* (2013) "Scanning space analysis in selective laser melting for CoCrMo powder," in *5th Manufacturing Engineering Society International Conference*. Zaragoza, pp. 370–378. doi: 10.1016/j.proeng.2013.08.228.

Qiu, C. *et al.* (2019) "On the solidification behaviour and cracking origin of a nickel-based superalloy during selective laser melting," *Materials Characterization*. Elsevier Inc., 148, pp. 330–344. doi: 10.1016/j.matchar.2018.12.032.

Roberts, I. A. (2012) *Investigation of residual stresses in the laser melting of metal powders in additive layer manufacturing*. PhD Thesis, University of Wolverhampton.

Robinson, J. *et al.* (2018) "Determination of the effect of scan strategy on residual stress in laser powder bed fusion additive manufacturing," *Additive Manufacturing*. Elsevier B.V., 23, pp. 13–24. doi: 10.1016/j.addma.2018.07.001.

Roehling, J. D. *et al.* (2019) "Reducing residual stress by selective large-area diode surface heating during laser powder bed fusion additive manufacturing," *Additive Manufacturing*. Elsevier, 28(May), pp. 228–235. doi: 10.1016/j.addma.2019.05.009.

Salmi, A. *et al.* (2017) "Experimental analysis of residual stresses on AlSi10Mg parts produced by means of selective laser melting (SLM)," *Procedia CIRP*. The Author(s), 62, pp. 458–463. doi: 10.1016/j.procir.2016.06.030.

Salmi, A. and Atzeni, E. (2017) "History of residual stresses during the production phases of AlSi10Mg parts processed by powder bed additive manufacturing technology," *Virtual and Physical Prototyping*. Taylor and Francis Ltd., 12(2), pp. 153–160. doi: 10.1080/17452759.2017.1310439.

Sames, W. J. *et al.* (2016) "The metallurgy and processing science of metal additive manufacturing," *International Materials Review*, pp. 1–46. doi: 10.1080/09506608.2015.1116649.

Sarkar, S., Kumar, C. S. and Nath, A. K. (2019) "Effects of different surface modifications on the fatigue life of selective laser melted 15–5 PH stainless steel," *Materials Science and Engineering A*. Elsevier B.V., 762(July), p. 138109. doi: 10.1016/j.msea.2019.138109.

Schajer, G. S. (2010) "Relaxation Methods for Measuring Residual Stresses: Techniques and Opportunities," *Experimental Mechanics*. Springer, 50(8), pp. 1117–1127. doi: 10.1007/s11340-010-9386-7.

Schajer, G. S. (2013) *Practical Residual Stress Measurement Methods*, *Practical Residual Stress Measurement Methods*. Edited by G. S. Schajer. Chichester, UK: John Wiley & Sons, Ltd. doi: 10.1002/9781118402832.

Schmeiser, F. *et al.* (2020) "Experimental observation of stress formation during selective laser melting using in situ X-ray diffraction," *Additive Manufacturing*. Elsevier B.V., 32, p. 101028. doi: 10.1016/j.addma.2019.101028.

Schneller, W. *et al.* (2019) "Effect of post treatment on the microstructure, surface roughness and residual stress regarding the fatigue strength of selectively laser melted AlSi10Mg structures," *Journal of Manufacturing and Materials Processing*, 3(4), p.

89. doi: 10.3390/jmmp3040089.

Shiomi, M. *et al.* (2004) “Residual stress within metallic model made by selective laser melting process,” *CIRP Annals*, 53(1), pp. 195–198. doi: 10.1016/S0007-8506(07)60677-5.

Simson, T. *et al.* (2017) “Residual stress measurements on AISI 316L samples manufactured by selective laser melting,” *Additive Manufacturing*. Elsevier B.V., 17, pp. 183–189. doi: 10.1016/j.addma.2017.07.007.

Song, B. *et al.* (2014) “Vacuum heat treatment of iron parts produced by selective laser melting: Microstructure, residual stress and tensile behavior,” *Materials and Design*. Elsevier Ltd, 54, pp. 727–733. doi: 10.1016/j.matdes.2013.08.085.

Song, J. *et al.* (2018) “Role of scanning strategy on residual stress distribution in Ti-6Al-4V alloy prepared by selective laser melting,” *Optik*. Elsevier GmbH, 170, pp. 342–352. doi: 10.1016/j.ijleo.2018.05.128.

Tal-Gutelmacher, E. and Eliezer, D. (2005) “High fugacity hydrogen effects at room temperature in titanium based alloys,” *Journal of Alloys and Compounds*, 404–406, pp. 613–616. doi: 10.1016/j.jallcom.2004.12.172.

Tong, Z. *et al.* (2019) “Laser additive manufacturing of FeCrCoMnNi high-entropy alloy: Effect of heat treatment on microstructure, residual stress and mechanical property,” *Journal of Alloys and Compounds*. Elsevier B.V, 785, pp. 1144–1159. doi: 10.1016/j.jallcom.2019.01.213.

Töppel, T. *et al.* (2016) “Eigenspannungen und verzug bei der additiven fertigung durch laserstrahlschmelzen,” *Schweissen und Schneiden*, 68(4), pp. 176–186.

Totten, G., Howes, M. and Inoue, T. (2002) *Handbook of Residual Stress and Deformation of Steel - ASM International*. ASM International. Available at: https://www.asminternational.org/search/-/journal_content/56/10192/06700G/PUBLICATION (Accessed: September 11, 2020).

Vrancken, B. *et al.* (2013) “Study of the influence of material properties on residual stress in selective laser melting,” in *Solid Freeform Fabrication Symposium*. Austin, pp. 393–407.

Vrancken, B. *et al.* (2014) “Residual stress via the contour method in compact tension specimens produced via selective laser melting,” *Scripta Materialia*, 87, pp. 29–32. doi: 10.1016/j.scriptamat.2014.05.016.

Vrancken, B. (2016) *Study of residual stresses in selective laser melting*. PhD Thesis, Katholieke Universiteit Leuven.

Walker, P. *et al.* (2019) “Effects of ultrasonic impact treatment on the stress-controlled fatigue performance of additively manufactured DMLS Ti-6Al-4V alloy,” *Applied Sciences (Switzerland)*, 9(22), pp. 12–14. doi: 10.3390/app9224787.

Wang, L. *et al.* (2018) “Investigation of performance and residual stress generation of AlSi10Mg processed by selective laser melting,” *Advances in Materials Science and Engineering*, 2018, pp. 1–12. doi: https://doi.org/10.1155/2018/7814039 Research.

Wang, M. *et al.* (2019) “Improved mechanical properties of AlSi7Mg/nano-SiCp composites fabricated by selective laser melting,” *Journal of Alloys and Compounds*. Elsevier Ltd, 810, p. 151926. doi: 10.1016/j.jallcom.2019.151926.

Wei, K. *et al.* (2019) “Effect of laser remelting on deposition quality, residual stress, microstructure, and mechanical property of selective laser melting processed Ti-5Al-2.5Sn alloy,” *Materials Characterization*. Elsevier, 150(October 2018), pp. 67–77. doi: 10.1016/j.matchar.2019.02.010.

Withers, P. J. and Bhadeshia, H. K. D. H. (2001a) “Residual stress part 1 - Measurement techniques,” *Materials Science and Technology*. IOM Communications Ltd., pp. 355–365. doi: 10.1179/026708301101509980.

Withers, P. J. and Bhadeshia, H. K. D. H. (2001b) “Residual stress part 2 - Nature and origins,” *Materials Science and Technology*. IOM Communications Ltd., pp. 366–375. doi: 10.1179/026708301101510087.

Wu, J., Wang, L. and An, X. (2017) “Numerical analysis of residual stress evolution of AlSi10Mg manufactured by selective laser melting,” *Optik*. Elsevier GmbH., 137, pp. 65–78. doi: 10.1016/j.ijleo.2017.02.060.

Xiao, Z. *et al.* (2020) “Effect of rescanning cycles on the characteristics of selective laser melting of Ti6Al4V,” *Optics and Laser Technology*. Elsevier Ltd, 122(October 2019), p. 105890. doi: 10.1016/j.optlastec.2019.105890.

Xu, R. *et al.* (2020) “Microstructure, metallurgical defects and hardness of Al–Cu–Mg–Li–Zr alloy additively manufactured by selective laser melting,” *Journal of Alloys and Compounds*. Elsevier Ltd, 835, p. 155372. doi: 10.1016/j.jallcom.2020.155372.

Yadroitsava, I. *et al.* (2015) *Residual stress in SLM Ti6Al4V alloy specimens*, *Materials Science Forum*. doi: 10.4028/www.scientific.net/MSF.828-829.305.

Yadroitsava, I. and Yadroitsev, I. (2015) “Residual stress in metal specimens produced by direct metal laser sintering,” in *Solid Freeform Fabrication Symposium*. Austin, pp. 614–625. doi: 10.1017/CBO9781107415324.004.

Yadroitsev, I. *et al.* (2013) “Energy input effect on morphology and microstructure of selective laser melting single track from metallic powder,” *Journal of Materials Processing Technology*, 213(4). doi: 10.1016/j.jmatprotec.2012.11.014.

Yadroitsev, I. and Yadroitsava, I. (2015) “Evaluation of residual stress in stainless steel 316L and Ti6Al4V samples produced by selective laser melting,” *Virtual and Physical Prototyping*. Taylor and Francis Ltd., 10(2), pp. 67–76. doi: 10.1080/17452759.2015.1026045.

Yan, M. *et al.* (2014) “A transmission electron microscopy and three-dimensional atom probe study of the oxygen-induced fine microstructural features in as-sintered Ti–6Al–4V and their impacts on ductility,” *Acta Materialia*. Acta Materialia Inc., 68, pp. 196–206. doi: 10.1016/j.actamat.2014.01.015.

Yasa, E. *et al.* (2009) “Investigation on occurrence of elevated edges in selective laser melting,” in *Solid Freeform Fabrication Symposium*. Austin. doi: 10.1017/CBO9781107415324.004.

Yu, W. *et al.* (2019) “Influence of re-melting on surface roughness and porosity of AlSi10Mg parts fabricated by selective laser melting,” *Journal of Alloys and Compounds*. Elsevier Ltd, 792, pp. 574–581. doi: 10.1016/j.jallcom.2019.04.017.

Zaeh, M. F. and Branner, G. (2010) “Investigations on residual stresses and deformations in selective laser melting,” *Production Engineering*, 4(1), pp. 35–45. doi: 10.1007/s11740-009-0192-y.

Zhang, B., Dembinski, L. and Coddet, C. (2013) “The study of the laser parameters and environment variables effect on mechanical properties of high compact parts elaborated by selective laser melting 316L powder,” *Materials Science and Engineering A*, 584, pp. 21–31. doi: 10.1016/j.msea.2013.06.055.

Zhang, C. *et al.* (2020) “Cracking mechanism and mechanical properties of selective laser melted CoCrFeMnNi high entropy alloy using different scanning strategies,” *Materials Science and Engineering A*. Elsevier Ltd, 789, p. 139672. doi: 10.1016/j.msea.2020.139672.

Zhang, M. *et al.* (2016) “Residual stress, defects and grain morphology of Ti-6Al-4V alloy produced by ultrasonic impact treatment assisted selective laser melting,” *Applied Sciences (Switzerland)*, 6(11), p. 304. doi: 10.3390/app6110304.

Zhao, L. *et al.* (2020) “Comparison of residual stresses obtained by the crack compliance method for parts produced by different metal additive manufacturing techniques and after friction stir processing,” *Additive Manufacturing*. Elsevier B.V., 36, p. 101499. doi: 10.1016/j.addma.2020.101499.

van Zyl, I., Yadroitsava, I. and Yadroitsev, I. (2016) “Residual stress in TI6AL4V objects produced by direct metal laser sintering,” *South African Journal of Industrial Engineering*, 27(4). doi: 10.7166/27-4-1468.